JGR Atmospheres

RESEARCH ARTICLE
10.1029/2025JD044444

Influence of Surface Aerosol Injection on Stratocumulus-to-Cumulus Transition: Cloud-Surface Coupling and Background Aerosol Concentrations

Haipeng Zhang[1,2], **Youtong Zheng**[3,4], **and Zhanqing Li**[1,2]

[1]Department of Atmospheric and Oceanic Science, University of Maryland, College Park, MD, USA, [2]Earth System Science Interdisciplinary Center, University of Maryland, College Park, MD, USA, [3]Department of Earth and Atmospheric Science, University of Houston, Houston, TX, USA, [4]Institute of Climate and Atmospheric Science, University of Houston, Houston, TX, USA

Abstract The influence of surface aerosol injection on the stratocumulus-to-cumulus transition (SCT) is explored using large-eddy simulations. We examine how cloud-surface coupling (or the strength of the marine boundary layer (MBL) stratification that limits vertical turbulent mixing and convection) impacts the vertical transport of aerosols, and how injected aerosols influence cloud properties and associated cloud radiative effects during the SCT. By injecting aerosols at different stages of the SCT, noting that cloud is more decoupled from the surface over time due to entrainment warming, we find that cloud-surface coupling significantly affects aerosol vertical transport. However, injection timing (before drizzle if any) does not notably affect the SCT and the efficiency of marine cloud brightening, because aerosol number concentrations due to injections at different times rapidly converge before the transition onset. By varying the background aerosol concentration, we find that injected aerosols can significantly extend the persistence of stratocumulus decks by suppressing precipitation in clean environments but have little impact on stratocumulus breakup with higher background aerosol concentrations due to saturated aerosol effects. In clean MBLs, the SCT-delay-induced increase in cloud fraction dominates the overall cooling effects in response to aerosols, followed by Twomey effects. These cooling effects are slightly offset by decreased liquid water path (LWP) due to entrainment drying. In polluted MBLs, the Twomey effect is more dominant, followed by cloud fraction adjustments, and these coolings are also partly offset by LWP adjustments. All the simulations are made in relatively small domains in which injected aerosols are homogenized over a short time scale.

Plain Language Summary Marine stratocumulus clouds exert strong radiative cooling on the Earth's climate. Deliberately injecting tiny airborne particles, known as aerosols, into the marine boundary layer (MBL) can brighten stratocumulus clouds by modifying cloud properties like cloud droplet size and the extent of cloud coverage, thereby enhancing their cooling effects. This study investigates marine cloud brightening (MCB) through Lagrangian large-eddy simulations. A stratocumulus-to-cumulus transition (SCT) case is adopted for the baseline simulation. By varying aerosol injection timing during the SCT, noting that cloud is more decoupled from the surface over time, we find that cloud-surface coupling significantly affects aerosol vertical transport. However, injection timing does not notably extend the SCT and influence the MCB efficiency, as aerosol number concentrations tend to converge rapidly prior to transition onset whenever aerosols are injected into MBL. Furthermore, we find that in clean environments aerosol injection markedly prolongs the presence of stratocumulus decks by suppressing precipitation; however, no significant delay occurs in polluted environments. The responses of cloud radiative effects also vary: in clean environments, cloud fraction adjustments dominate MCB, whereas in polluted environments, albedo effects are more influential. These findings have significant implications for the geoengineering strategies of MCB.

Key Points:

- Cloud-surface coupling significantly influences aerosol vertical transport during the stratocumulus-to-cumulus transition (SCT)
- Aerosol injection timing does not notably affect the SCT and the efficiency of marine cloud brightening (MCB)
- MCB is more efficient when aerosols are injected into a clean environment and delay the onset of strong precipitation

Supporting Information:

Supporting Information may be found in the online version of this article.

Correspondence to:

Z. Li and Y. Zheng,
zhanqing@umd.edu;
yzheng18@uh.edu

Citation:

Zhang, H., Zheng, Y., & Li, Z. (2026). Influence of surface aerosol injection on stratocumulus-to-cumulus transition: Cloud-surface coupling and background aerosol concentrations. *Journal of Geophysical Research: Atmospheres*, *131*, e2025JD044444. https://doi.org/10.1029/2025JD044444

Received 27 MAY 2025
Accepted 14 DEC 2025

1. Introduction

Stratocumulus clouds cover a quarter of the ocean's surface. Due to the extensive area coverage and low altitude, they effectively reflect sunlight and cool the Earth's surface (Hartmann & Short, 1980; Klein & Hartmann, 1993). A small change in the coverage of stratocumulus clouds can substantially alter the amount of heat the Earth retains (Slingo, 1990). It is therefore important to understand the behavior of these clouds. One poorly understood phenomenon about stratocumulus clouds is how they transition to cumulus clouds, called the stratocumulus-to-cumulus transition (SCT).

The SCT is characterized by the marine boundary layer (MBL) evolving from an initial state of a well-mixed layer topped with an overcast stratocumulus cloud deck capped by a strong inversion into a deeper and more decoupled and desiccated layer dominated by cumulus clouds under a weaker inversion (Albrecht et al., 1995, 2019; Bretherton et al., 1999; Wyant et al., 1997). This transition is prevalent over the subtropics (Scott et al., 2020; Zhang et al., 2024), where stratocumulus clouds are advected toward warmer water by trade winds (or experience cold-air advection). The SCT is influenced by various background meteorological factors. A larger estimated inversion strength in the background prolongs the persistence of initial overcast stratocumulus decks during the SCT (Eastman & Wood, 2018). This occurs because a stronger cloud-top inversion traps more moisture in the MBL, delaying the breakup of the stratocumulus decks (Bretherton et al., 2013; Zhang et al., 2024). In contrast, increased background sea surface temperature (SST) accelerates the SCT, as it enhances the buoyancy-driven mixing of dry air from the free troposphere (FT) into the MBL, more efficiently drying the clouds through entrainment (known as entrainment drying) (Deardorff, 1976; Igel, 2024; Rieck et al., 2012; Wood & Bretherton, 2004; Zhang et al., 2024). Similarly, stronger background subsidence accelerates the transition by drawing more dry air downward from the FT (Sandu & Stevens, 2011; van der Dussen et al., 2016; Zhang et al., 2023).

Besides meteorological factors, aerosols have a significant role in stratocumulus clouds as well. Adding aerosols into the atmosphere, such as anthropogenic pollution or volcanic eruptions, increases cloud condensation nuclei (CCN), yielding more numerous and smaller cloud droplets given a fixed liquid water path (LWP), resulting in cloud brightening (the Twomey effect; Twomey, 1977). However, the responses of cloud macrophysical properties (cloud fraction and LWP) to CCN, known as cloud adjustments, remain highly uncertain. For a precipitating stratocumulus-topped boundary layer (STBL), increasing CCN would reduce cloud droplet size, which decreases collision-coalescence efficiency, consequently suppressing precipitation and increasing LWP and cloud cover (Albrecht, 1989). For a weak- or non-precipitating STBL, LWP responses to increased aerosols are governed by the interplay between moistening due to decreased surface precipitation and drying from enhanced cloud-top entrainment (Ackerman et al., 2004). The enhanced entrainment is caused by the sedimentation-entrainment effect (Ackerman et al., 2004; Bretherton et al., 2007) or enhanced radiative-cooling-driven entrainment induced by a dependence of the maximum radiative cooling rate on cloud effective radius (Williams & Igel, 2021). In that regard, when dry air overlies the MBL, LWP likely decreases in response to increasing aerosols. Considering the crucial role of aerosols in altering cloud properties, it is therefore necessary to investigate the aerosol effects on the SCT.

Large-eddy simulations (LESs) can resolve fine-scale processes like entrainment and MBL turbulence, enabling a process-level understanding of aerosol-cloud interactions (ACI). The impact of aerosols on marine clouds have been investigated by injecting aerosols from the surface to MBL via LESs (Berner et al., 2015; Chun et al., 2023; Wang et al., 2011). Such an aerosol perturbation is designed to mimic natural experiments such as ship emissions and pollution plumes (Christensen et al., 2022). This design not only helps enhance the mechanistic understanding of ACI but may also help inform the development of strategies for a climate intervention approach, commonly referred to as marine cloud brightening (MCB). That is, intentionally introducing CCN into subtropical low marine clouds to increase cloud albedo and mitigate global warming (Latham, 1990), motivated by the sensitivity of clouds to aerosols (e.g., the Twomey effect). For example, Wang et al. (2011) performed a series of aerosol-injection experiments in a stratocumulus simulation case, revealing that cloud adjustments and associated albedo perturbation strongly depend on the background meteorological conditions and aerosol number concentrations. Their findings highlighted the effectiveness of MCB through aerosol injection into a weakly precipitating MBL or a CCN-limited MBL that follows heavy precipitation events. Similarly, Chun et al. (2023) comprehensively examined the responses of cloud properties and cloud radiative effects (CREs) to surface aerosol injection, demonstrating that aerosol injection generally brightens shallow marine clouds via the Twomey effect. This brightening is enhanced by positive LWP adjustments in a clean MBL with strong drizzle but offset by negative LWP adjustments in moderate and polluted MBLs. More recently, Prabhakaran et al. (2024) have investigated the role of aerosol forcings in the SCT, confirming MCB in response to aerosol injection in both pristine and polluted environments. They also determined that the relative contribution from the Twomey effect and cloud adjustments to brightening varies depending on simulation time and background aerosols.

However, most LES studies concerning surface aerosol injection have been based on fixed meteorological conditions and short simulation durations (e.g., Chun et al., 2023; Dhandapani et al., 2025; Possner et al., 2018; Wang et al., 2011), with few considering the evolution of boundary conditions that are more realistic (e.g., Prabhakaran et al., 2024). Moreover, an important physical process, cloud-surface coupling, has been

overlooked in previous LES studies of MCB. This coupling of clouds with the surface has been shown to significantly influence the vertical transport of near-surface moisture (Zhang et al., 2023; Zheng et al., 2021), expected so for the vertical transport of surface aerosols, thereby impacting MCB efforts. Therefore, further studies of aerosol effects on the SCT are needed to enhance our understanding of ACI. In this study, we aim to understand the response of clouds to aerosol injection based on a realistic SCT case by addressing the following questions:

1. How does cloud-surface coupling affect the vertical transport of surface aerosols during the SCT?
2. Does aerosol injection timing influence the SCT and the efficiency of MCB?
3. What are the influences of aerosol injection on cloud properties and CREs during the SCT and associated dependence on background aerosol concentrations?

Section 2 introduces the LES model used, and modeling experiments, and a method of analyzing the LWP budget. Sections 3–5 present the findings that address the above three questions. The discussion and summary are given in Section 6 and 7, respectively.

2. Methodology

2.1. LES Model

The LES model used is version 6.11.3 of the System for Atmospheric Modeling (SAM), originally developed by Khairoutdinov and Randall (2003). In SAM, subgrid-scale turbulence is handled using a 1.5-order subgrid-scale turbulent kinetic energy scheme (Deardorff, 1980). Radiation is represented by the RRTMG scheme (Iacono et al., 2008). The model also incorporates the two-moment Morrison microphysics scheme (Morrison & Grabowski, 2008) coupled with a bulk aerosol scheme (Berner et al., 2013), enabling simulations of the aerosol life cycle and providing a more realistic representation of aerosol-cloud-precipitation interactions. The microphysics scheme predicts both the number concentrations and mixing ratios of cloud and rain droplets. Condensation is determined through saturation adjustment when the water vapor mixing ratio exceeds the saturation mixing ratio. Evaporation of drizzle is explicitly represented, while vapor deposition onto drizzle is not.

The bulk aerosol scheme predicts the number and mass mixing ratios of single accumulation-mode aerosols in three categories: unactivated, cloud-borne, and rain-borne (Berner et al., 2013). It represents the processes of activation, autoconversion, accretion, evaporation, interstitial scavenging, surface sources, and sedimentation. The aerosol is assumed to be fully soluble within condensate and reappears as a single particle when the cloud or raindrop evaporates. The number and mass fluxes of sea salt aerosol spray are determined by wind speeds following Clarke et al. (2006), where the size-resolved fluxes are refit using a single, lognormal accumulation mode with a geometric mean diameter of 160 nm. Cloud droplets are activated from aerosol particles of this lognormal aerosol size distribution. In the free troposphere, the aerosol geometric mean diameter is specified as 120 nm.

2.2. Experimental Design

A set of LES simulations are conducted to represent the evolution of an air mass for several tens of hours downstream with aerosols injected briefly during this period. These simulations are based on a Lagrangian trajectory selected from the Cloud System Evolution in the Trade field campaign, which took place in July 2015 over Northeast Pacific (Albrecht et al., 2019). This trajectory begins with a clean, well-mixed STBL, and relatively strong precipitation, followed by a clear SCT (see L06 case in Figure 1 from Erfani et al. (2022b)). This SCT case has been set up, simulated, and evaluated by Erfani et al. (2022b) using SAM. We generally follow their settings to conduct the baseline simulation (named CTL). It runs for 72 hr, starting from 01 UTC 17 July 2015. The radiation is calculated every 15 s. These simulations are conducted within a doubly periodic domain of 10.8×10.8 km^2. The horizontal resolution is set to 100 m, while the vertical grid spacing varies, starting from 25 m near the surface and decreasing to 10 m between 950 and 3,800 m in height. Beyond this range, the vertical grid spacing gradually increases to 60 m, with a total of 432 vertical layers. The forcing data, including geostrophic winds, large-scale vertical velocity, and SSTs, are obtained from ERA5 reanalysis (Hersbach et al., 2020). Compared to MERRA2 reanalysis (Gelaro et al., 2017), the large-scale vertical velocity from ERA5 agrees better with the aircraft dropsonde measurement (Li et al., 2022). Initial temperature and moisture profiles are based on aircraft data in the MBL and ERA5 above. Time-varying vertical profiles of accumulation mode

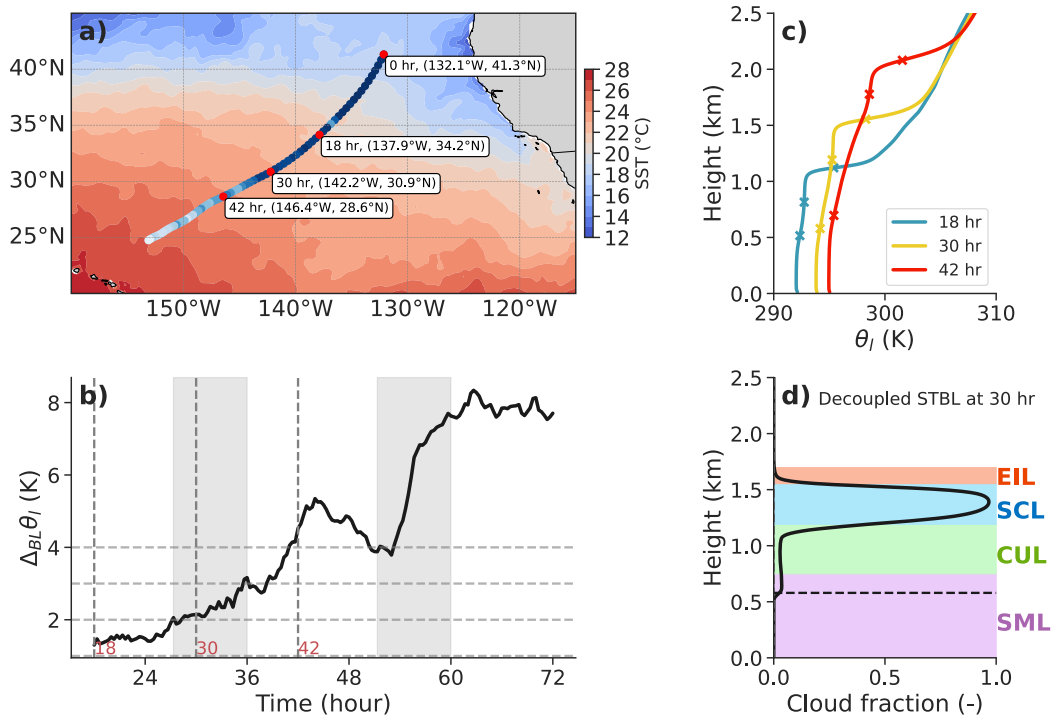

Figure 1. (a) 72-hr trajectory of the stratocumulus-to-cumulus transition for simulations. Along the trajectory, the shading from dark to white denotes the cloud fraction ranging from 1 to 0. The annotation of "0 hr" marks the starting time (01 UTC 17 July 2015) and location of the trajectory, while the other three indicate the times and locations of the injection experiments, INJ18, INJ30, and INJ42, respectively. The background map shows the spatial distribution of sea surface temperature. (b) Time series of the decoupling degree or the marine boundary layer (MBL) stability ($\Delta\theta_l$) for the CTL run. $\Delta\theta_l$ is defined as the θ_l averaged over the top 10% of MBL minus the θ_l averaged over the bottom 10% of MBL, where θ_l is liquid water potential temperature. Gray boxes mark nighttime (7 p.m.–4 a.m. Local Time). (c) Vertical profiles of θ_l at 18 hr, 30 hr, and 42 hr from the CTL run. Symbols "x" from bottom to top represent the lifted condensation level (LCL), and cloud-base and cloud-top heights of the stratocumulus cloud deck. (d) Schematic diagram illustrating the structure of a decoupled stratocumulus-topped boundary layer, including the entrainment layer (EIL), stratocumulus layer (SCL), shallow cumulus layer (CUL), and surface mixed layer (SML). The dashed line denotes the LCL.

aerosol number concentration (N_{Ac}) (including dry/unactivated aerosols and cloud-borne aerosols), derived from MERRA2, are used to initialize the MBL N_{Ac} and force the FT N_{Ac}. More details on input data can be found in Erfani et al. (2022b). For the first 18 hr, temperature and water mixing ratio profiles are nudged to aircraft observations every 3 hr to enable the LES to develop a well-mixed MBL. Afterward, temperature, moisture, and aerosol evolve freely within the MBL. Throughout the simulation, these variables in the FT are nudged to a combination of observations and ERA5 above 500 m from the inversion.

To address the first question, we conduct three sensitivity runs (INJ18, INJ30, and INJ42), each involving a single aerosol injection at the surface based on the CTL run, occurring at the 18th, 30th, and 42nd hr of the simulation, respectively. Such a design is motivated by the fact that stratocumulus decks are gradually decoupled from the surface due to entrainment warming during the SCT (Bretherton & Wyant, 1997), yielding an evolution in the degree of decoupling over time (Figure 1b), helping understand the impact of decoupling on aerosol vertical transport. At the time of interest, we inject 200 nm-diameter aerosol particles using a point sprayer placed at the surface, operating at an injection rate of 1×10^{16} particles per second. This injection rate is comparable to those used in previous studies (Chun et al., 2023; H. Wang et al., 2011; Wood, 2021). The sprayer moves at a domain-relative speed of 4.5 m/s for 2133 s, allowing traveling once through the domain (see sprayer trajectories in Figure S1 of Supporting Information S1). These sensitivity runs will also help address the second question.

The third question regarding the aerosol effects on the SCT is addressed by contrasting the INJ18 run with the CTL run. To further evaluate the effect of aerosol injection rates on the SCT, we double the injection rate in INJ18 to 2×10^{16} no./s, named INJ18_2X. The impacts of polluted backgrounds are examined by tripling the initial N_{Ac}

Table 1
Summary of Conditions Used for Running Sensitivity Experiments

Objective	Run ID	Description	Injection rate (no./s)
Baseline conditions	CTL	Control run, with initial N_{Ac} and FT N_{Ac} derived from MERRA2	–
	POL	Polluted run by tripling initial N_{Ac} and FT N_{Ac} in CTL	–
Impact of cloud-surface coupling on aerosol vertical transport and the role of injection timing in the SCT	INJ18 (INJ18POL)	Inject aerosols at 18 hr in CTL (POL)	1×10^{16} (3×10^{16})
	INJ30 (INJ30POL)	Inject aerosols at 30 hr in CTL (POL)	1×10^{16} (3×10^{16})
	INJ42 (INJ42POL)	Inject aerosols at 42 hr in CTL (POL)	1×10^{16} (3×10^{16})
Impact of aerosol effects on the SCT	INJ18	Same as above, used for a different purpose	1×10^{16}
	INJ18_2X	Double the injection rate of INJ18	2×10^{16}
The role of polluted background	INJ18POL	Polluted version of INJ18	3×10^{16}
	INJ18POL_2X	Polluted version of INJ18_2X	6×10^{16}

and FT N_{Ac} for CTL, INJ18, and INJ18_2X, resulting in polluted simulation sets, POL, INJ18POL, and INJ18POL_2X. The injection rates for INJ18POL and INJ18POL_2X are also tripled compared to their clean counterparts to maintain a similar fractional change in the MBL-average N_{Ac} between the CTL and POL scenarios. The MBL average is calculated as the air-density-weighted average of a variable from surface to inversion. The conditions for running all sensitivity experiments are summarized in Table 1.

2.3. LWP Budget Analysis

To explore how physical processes affect the SCT transition, we use a LWP budget analysis developed by van der Dussen et al. (2014):

$$\frac{\partial \mathrm{LWP}}{\partial t} = \underbrace{\rho w_e \left(\eta \Delta q_t - \Pi \gamma \eta \Delta \theta_l - h \Gamma_{q_l}\right)}_{\text{Entrainment}} + \underbrace{\rho \eta \left(\overline{w' q_t'}(z_b) - \Pi \gamma \overline{w' \theta_l'}(z_b)\right)}_{\text{Cloud-base tubulent fluxes}} + \underbrace{\frac{\eta \gamma}{c_p} \cdot \left(F_{\mathrm{rad}}(z_t) - F_{\mathrm{rad}}(z_b)\right)}_{\text{Radiation}}$$
$$+ \underbrace{\left(-\rho (P(z_t) - P(z_b))\right)}_{\text{Precipitation}} + \underbrace{\left(-\rho h \Gamma_{q_l} w_{\mathrm{sub}}\right)}_{\text{Subsidence}} + \underbrace{\epsilon}_{\text{Residual}} \quad (1)$$

where ρ is the air density (kg/m^3), w_e the entrainment rate (m/s), Π the Exner function, h the cloud thickness (m), q_t the total water mixing ratio (kg/kg), and θ_l the liquid water potential temperature (K). z_b and z_t are the cloud-base and cloud-top heights (m), respectively, while Γ_{q_l} (kg/kg/m) denotes the lapse rate of the liquid water mixing ratio q_l (kg/kg). The radiative flux (F_{rad}, W/m^2) and precipitation flux (P, m/s) are both negative downward. $\overline{w' q_t'}(z_b)$ and $\overline{w' \theta_l'}(z_b)$ represent the moisture flux (kg/kg m/s) and the heat flux (K m/s) at the cloud base, respectively, while w_{sub} denotes the large-scale subsidence rate (m/s) at the MBL top. The parameter $\gamma = \frac{\partial q_s}{\partial T}$ (g/kg/K) is the change of the saturation specific humidity q_s (g/kg) with temperature T in the cloud layer, derived from the Clausius-Clapeyron relationship. The thermodynamic factor η is a defined as $\left(1 + \frac{L_v \gamma}{c_p}\right)^{-1}$, where L_v is the latent heat of vapourization (J/kg), and c_p is the specific heat of air at constant pressure (J/kg/K). Finally, Δq_t and $\Delta \theta_l$ indicate the inversion jumps of moisture and temperature, respectively. The five forcing terms on the right-hand side of Equation 1 correspond to the rate of LWP changes contributed by entrainment (*Ent*) leading to evaporation due to entrainment drying, turbulent fluxes at the cloud base (*Base*) leading to turbulent moistening, radiation (*Rad*) leading to condensation due to radiative cooling, precipitation (*Prec*) leading to LWP depletion, and subsidence (*Subs*) leading to evaporation due to bringing dry air downward, respectively. The residual of the LWP tendency decomposition is $\epsilon = \frac{\partial \mathrm{LWP}}{\partial t}\big|_{\mathrm{mod}} - Ent - Base - Rad - Prec - Subs$, where $\frac{\partial \mathrm{LWP}}{\partial t}\big|_{\mathrm{mod}}$ is the actual total LWP tendency. More details of the physical processes are described in Zhang et al. (2023). Note that LWP budget analyses are based on domain-mean values.

2.4. Decomposition of CRE Changes

To understand how aerosols affect CRE at the process level, changes in CRE (dCRE) due to aerosol perturbations can be decomposed into contributions from the Twomey effect ($dCRE_{N_c}$), LWP adjustments ($dCRE_{LWP}$), and cloud fraction adjustments ($dCRE_{CF}$). Following the methodology proposed by Chun et al. (2023) and Diamond et al. (2020), dCRE is decomposed as:

$$\begin{aligned} dCRE = &\underbrace{F_{in}\cdot CF_{ctl}\left(A_{cld,N_c}-A_{cld,ctl}\right)}_{dCRE_{N_c}} + \underbrace{F_{in}\cdot CF_{ctl}\left(A_{cld,LWP}-A_{cld,ctl}\right)}_{dCRE_{LWP}} \\ &+ \underbrace{F_{in}\cdot (CF_{pl}-CF_{ctl})(A_{cld,pl}-A_{clr})}_{dCRE_{CF}} + \underbrace{\zeta}_{Residual}, \end{aligned} \tag{2}$$

where F_{in} is solar insolation; $A_{cld,ctl/pl}$ is the cloud albedo for the control or plume run; $CF_{ctl/pl}$ is low-cloud fraction (LCF) for the control or plume run; A_{clr} is the clear-sky albedo. $(A_{cld,N_c} - A_{cld,ctl})$ represents the change in cloud albedo in the plume run relative to control that is associated with the change in cloud droplet number concentration (N_c), and the impact of in-cloud LWP changes are defined analogously. Note that plume areas in the plume run may not cover the whole domain. To take the area fraction of plumes (AF_{pl}) into account, dCRE needs to be separately calculated in the plume areas and the background and then weight-averaged by their respective area fractions. In our study, due to a small domain ($\sim 10 \times 10$ km^2) used, the aerosols are efficiently mixed horizontally and able to fill the whole domain within ~2 hr once injected (Figure S2 in Supporting Information S1) and persist throughout the simulations. Therefore, in our study, $AF_{pl} \approx 1$ in the plume run, which simplifies dCRE decomposition calculation. We acknowledge that adopting a small domain precludes mesoscale circulation's impact on aerosol mixing and tends to delay precipitation onset and the SCT compared to larger domains (Yamaguchi et al., 2017). We still favor it because this setting allows us to focus on the decoupling's influence on aerosol vertical transport on a large-eddy scale, the core of our study, and meanwhile, the simulated LWP in the control case is even closer to observations than that from larger domains (25.6×25.6 km^2) (Erfani et al., 2022b). The accuracy of dCRE decomposition can be examined by checking the residual of the budget, $\zeta = dCRE_{mod} - dCRE_{N_c} - dCRE_{LWP} - dCRE_{CF}$, where $dCRE_{mod}$ is the LES-modeled dCRE.

3. Role of Cloud-Surface Coupling in Aerosol Vertical Transport

Figure 2 compares the evolution of N_{Ac} profiles when aerosols are injected into the MBL at different times. The analyses in this study are based on domain averages unless otherwise stated. When aerosols are injected at 18 hr (i.e., INJ18), the MBL is weakly decoupled, or cumulus coupled (Figure 1c). After injection, aerosols remain nearly well-mixed within the surface mixed layer or subcloud layer (below the lifted condensation level) (Figure 2b or Figure 3a), but the cumulus layer above that is stratified due to entrainment warming (Bretherton & Wyant, 1997) and limits further turbulent mixing and upward transport. At this stage, part of the aerosols is detrained into the cumulus layer as updrafts rise. Some aerosols can be further transported into the stratocumulus layer through cumulus updrafts. Within the stratocumulus layer, turbulent motions efficiently mix the aerosols below the cloud-top inversion. When aerosols are injected at 30 hr (i.e., INJ30), the majority of aerosols are also trapped below 0.5 km within the subcloud layer (Figures 1c and 2c). But the cumulus layer at 30 hr becomes more stratified, which increasingly hampers the upward transport of aerosols. As a result, the N_{Ac} that reaches the cloud layer is significantly reduced compared to the INJ18 run. A more remarkable suppression of aerosol vertical transport is noticed in the INJ42 run, manifested by a clear gradient jump of the N_{Ac} in the lower MBL and the fewer aerosols entered into the cloud layer (Figure 2d). The decoupling or stability of the MBL, therefore, demonstrates a marked influence on aerosol vertical mixing, which might affect the efficiency of MCB through surface aerosol injection.

Further details of aerosol vertical transport are shown in Figure 3, which presents the profiles of the domain-mean, in-cloud, and in-core (buoyant-updraft core) aerosols, along with in-core updrafts and core area fraction over the whole domain 2 hours after injection. Two hours allow aerosols to be homogenized horizontally after injection. Overall, aerosols are relatively well mixed within the subcloud and stratocumulus layers (Figure 3a). In contrast, within the cumulus layer, the in-cloud and particularly the in-core aerosol concentrations are much closer to those in the subcloud layer (Figures 3b and 3c) and considerably larger than the domain-mean concentrations. These features clearly indicate that cumulus updrafts serve as a pathway for aerosol transport in a decoupled MBL.

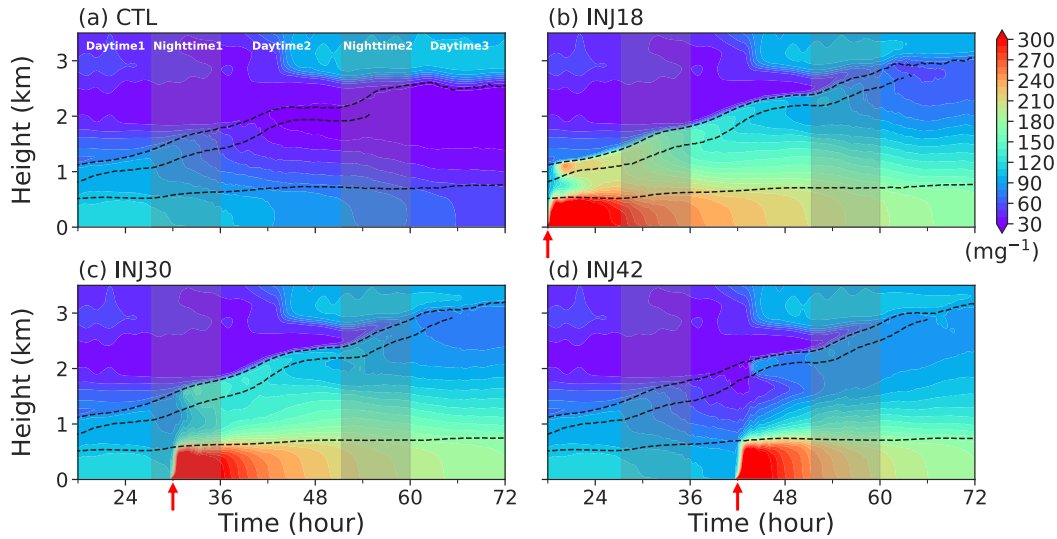

Figure 2. Time-height cross sections of accumulation mode aerosol number concentration (dry aerosols plus cloud-borne aerosols; N_{Ac}) for simulations (a) CTL, (b) INJ18, (c) INJ30, and (d) INJ42. Gray boxes mark nighttime (7 p.m.–4 a.m. Local Time). The dashed lines represent the stratocumulus cloud-top and cloud-base heights, and the lifted condensation level, respectively.

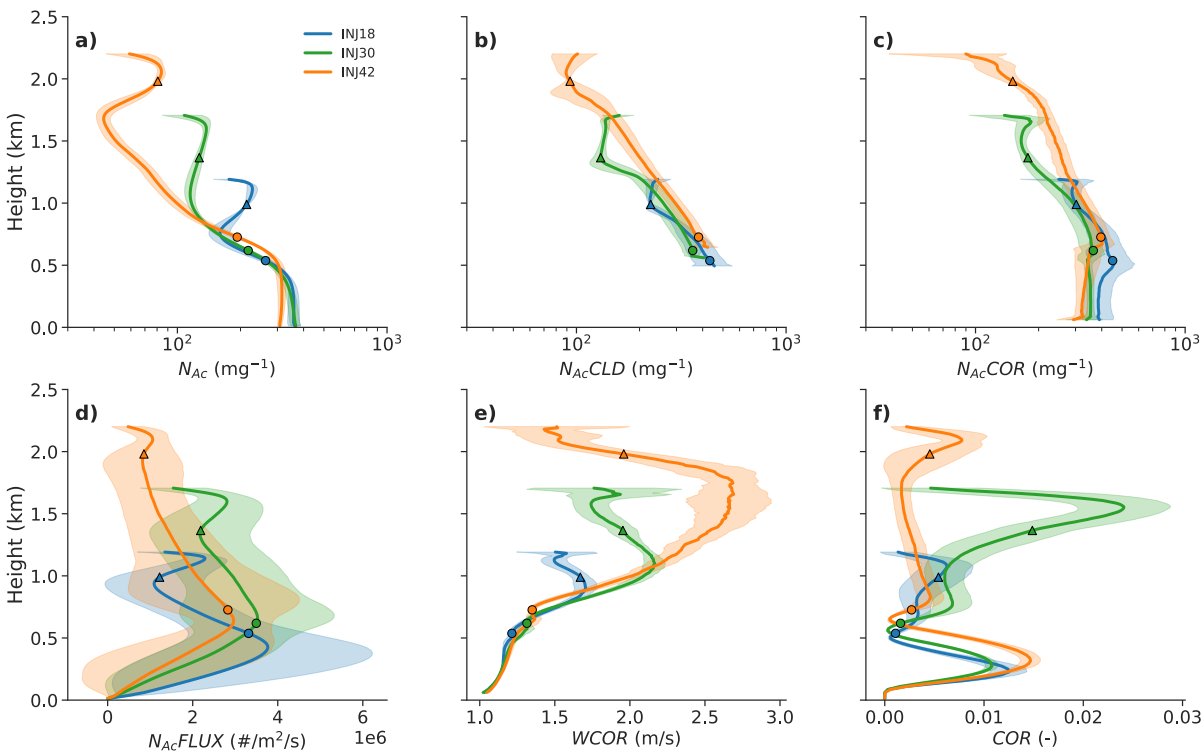

Figure 3. Vertical profiles (up to the inversion height) of accumulation mode aerosol number concentration (N_{Ac}), averaged from 2 to 5 hours after injection, for experiments INJ18 (blue), INJ30 (green), and INJ42 (orange). Panels (a–c) show N_{Ac} averaged over the whole domain, in the cloud, and in the buoyant updraft core, respectively. Panels (d–f) display the domain-mean N_{Ac} fluxes, the in-core vertical velocity, and the buoyant updraft core fraction over the whole domain, respectively. The shading denotes the standard deviation of each line, derived from nine 20-min-average samples over the three-hour period. Dots and triangles indicate the heights of lifted condensation level and stratocumulus cloud base, respectively.

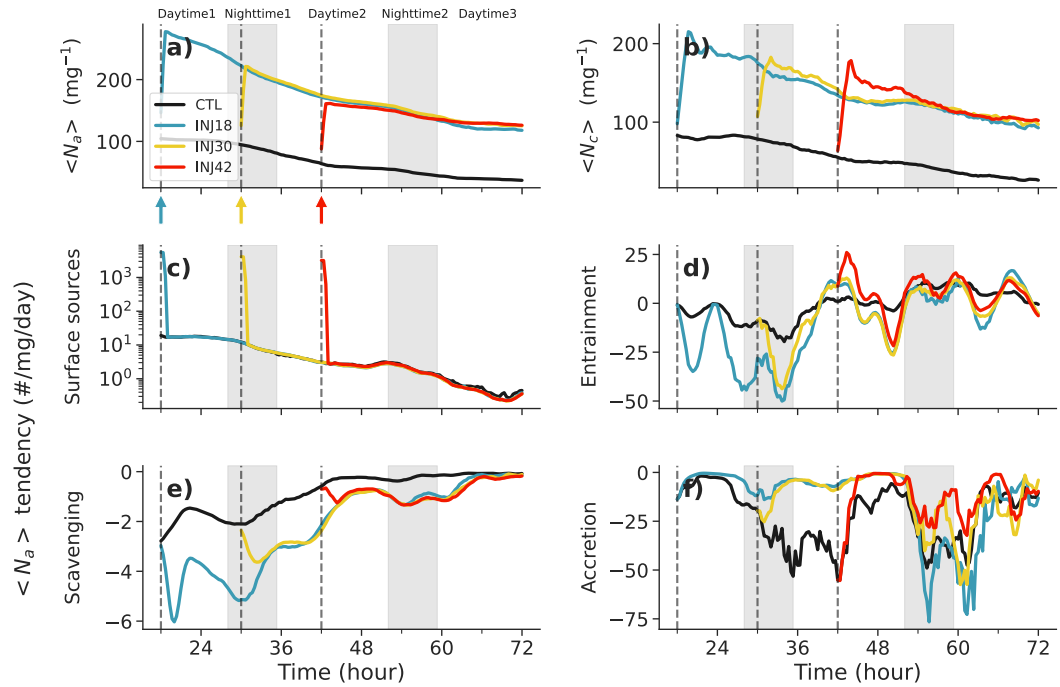

Figure 4. Time series of (a) MBL-average total aerosol number concentration (including dry, cloud-borne, and rain-borne aerosols) ($<N_a>$) and (b) MBL-average in-cloud N_c for the CTL run and three plume runs (INJ18, INJ30, and INJ42). Panels (c–f) show selected MBL-average aerosol budget tendencies for N_a due to surface fluxes, cloud-top entrainment of free-tropospheric air, scavenging, and accretion, respectively. Gray boxes mark nighttime (7 p.m.–4 a.m. Local Time).

The domain-mean N_{Ac} in the stratocumulus layer decreases markedly with later aerosol injections (Figure 3a). To understand this reduction, we examine how vertical aerosol transport changes as the MBL becomes increasingly decoupled from INJ18 to INJ42. Relative to the earlier injection (INJ18), the later injection runs (INJ30 and INJ42) show weaker N_{Ac} fluxes in the surface mixing layer as the MBL stabilizes (Figure 3d), resulting in fewer aerosols reaching the stratocumulus cloud base and hence lower N_{Ac} in the stratocumulus layer (Figure 3a). Among the later injection runs, cumulus updrafts in INJ42 become substantially stronger than in INJ30 due to enhanced surface fluxes (Figure 3e), which allows aerosols to be lofted more efficiently (Figures 3b and 3c) and to higher altitudes within the cloud (Figure S3 in Supporting Information S1). However, the buoyant updraft core area fraction near the stratocumulus cloud base decreases substantially in INJ42 (Figure 3f) due to stronger stratification in the cumulus layer, offsetting the benefit of stronger updrafts and limiting overall aerosol transport efficiency compared to INJ30 (Figure 3d). Thus, a more decoupled MBL inhibits aerosol transport to the stratocumulus base through two dynamical ways: weakening the MBL turbulent mixing and reducing the fractional area of buoyant updraft cores within the cumulus layer. In addition to these ways, the decrease in the N_{Ac} in the stratocumulus layer is also partly because the same number of aerosol particles becomes more diluted when distributed throughout a deeper boundary layer at later injection times.

4. Implication of Aerosol Injection Timing for the SCT and MCB Efficiency

Section 3 demonstrates that increasing MBL decoupling with time substantially limits aerosol vertical transport, resulting in fewer aerosols reaching the cloud layer. This raises an important question: since decoupling suppresses upward transport, would injecting aerosols earlier, when the MBL is relatively coupled, enhance the amount of aerosols available to influence the SCT and the overall MCB efficiency (equivalent to the second question)? We will address it in this section.

Figure 4 illustrates the time series of aerosol budget tendencies of total aerosol number concentration (including dry/unactivated, cloud-borne, and rain-borne aerosols), $<N_a>$ ("< >" means MBL-average), from the three plume runs (INJ18, INJ30, and INJ42), showing how injection timing impacts aerosol evolution in the MBL.

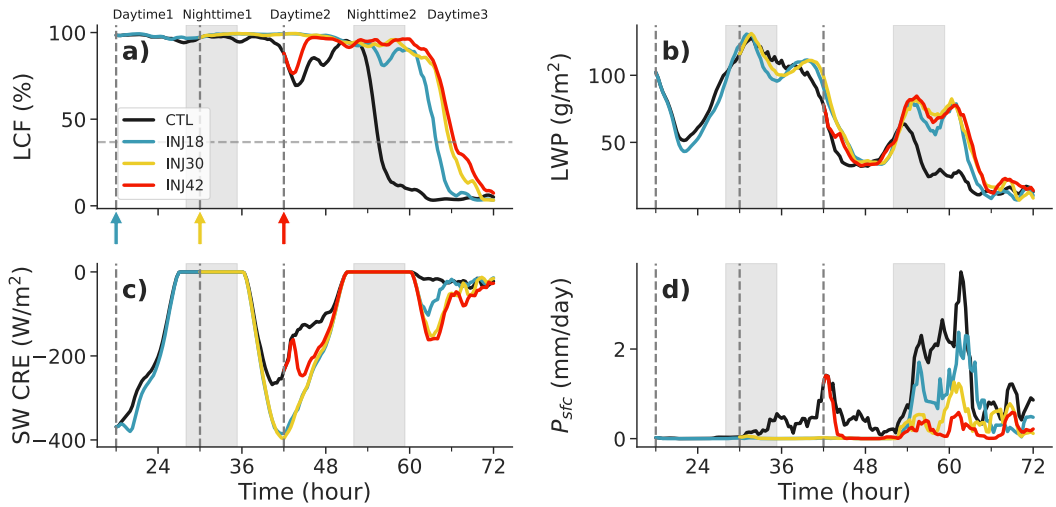

Figure 5. Time series of domain-mean (a) low-cloud fraction (LCF), (b) liquid water path, (c) shortwave cloud radiative effect, and (d) surface precipitation rate for experiments CTL, INJ18, INJ30, and INJ42. Gray boxes mark nighttime (7 p.m.–4 a.m. Local Time). The horizontal dashed line in panel (a) represents the value to which the initial LCF decreases by a factor of e.

Broadly, the evolution of $<N_a>$ is mainly controlled by surface aerosol fluxes (source term), cloud-top entrainment (source or sink terms), interstitial scavenging (sink term), and accretion (sink term), which is also true for $<N_c>$, showing the similar evolution patterns. Other processes like autoconversion and sedimentation are not shown due to their negligible impacts. When aerosols are injected at 18 hr, surface aerosol fluxes exhibit a sharp spike, followed by a rapid decrease to their pre-injection state (Figure 4c). This injection gives rise to a roughly tripled $<N_a>$ and a doubled $<N_c>$ upon aerosol injection relative to the CTL run (Figures 4a and 4b). Over the subsequent 12 hr, $<N_a>$ decreases more sharply compared to CTL, primarily due to drastically enhanced entrainment dilution (Figure 4d) as a result of increased aerosol gradient between the MBL and FT (Figure 2b). Strengthened interstitial scavenging also contributes, albeit to a much lesser extent (Figure 4e). During the second 12 hr after injection, the rate of decline in $<N_a>$ slows down, because increased aerosols suppress the drizzle during this period (Figure 5d), and the consequent reduction in the accretion of cloud water by raindrops (Figure 4f) effectively counterbalances the enhanced aerosol dilution by entrainment. One day after the injection, the decline rate of $<N_a>$ resembles that of CTL, as demonstrated by their parallel time series in Figure 4a. This is possibly caused by no notable perturbation of the aerosol entrainment term. It is worth noting that, later in simulations, the contribution of entrainment processes to $<N_a>$ reverses to be positive because reduced N_a in the MBL, removed by enhanced drizzle or accretion processes, becomes smaller than background FT N_a (Figure 2a).

When aerosols are injected later (more decoupled MBL), the resulting peak of $<N_a>$ is notably lower (see INJ30 and INJ42 in Figure 4a). Intriguingly, these lowered peaks in INJ30 and INJ42 fall almost into the declining line of $<N_a>$ in INJ18. This alignment suggests that the aerosol removal by entrainment and accretion over the SCT are close to the aerosol supply reduction induced by MBL decoupling, which inhibits the injection of surface aerosols into the MBL. Furthermore, the subsequent declining lines of $<N_a>$ for INJ30 and INJ42 are overlapped with that in INJ18. These features hold for $<N_c>$ within the cloud as well. Despite a short overshooting after injection, the evolution of the $<N_c>$ in INJ30 and INJ42 ultimately converges to the declining line of that in INJ18 (Figure 4b).

The convergence of $<N_a>$ evolution is attributed to the convergence observed in the aerosol budget terms. Although these budget terms converge overall, the timescale of convergence varies under different conditions. Specifically, for the entrainment term, the $<N_a>$ tendency in INJ30 converges with that in INJ18 within 3 hr, whereas it takes about 9 hr for INJ42 (Figure 4d). The slower adjustment timescale in INJ42 is likely because of the weaker cloud-top radiative cooling during the daytime and the stratocumulus cloud fraction falling below 100% at the time of injection (Y. S. Chen et al., 2025). For the scavenging and accretion terms, both INJ30 and INJ42 show rapid convergence (within 3 hr). The convergence of the accretion term beyond 54 hr in INJ30 and INJ42 is, however, uncertain, possibly due to the high susceptibility of precipitation to aerosols. The consistent

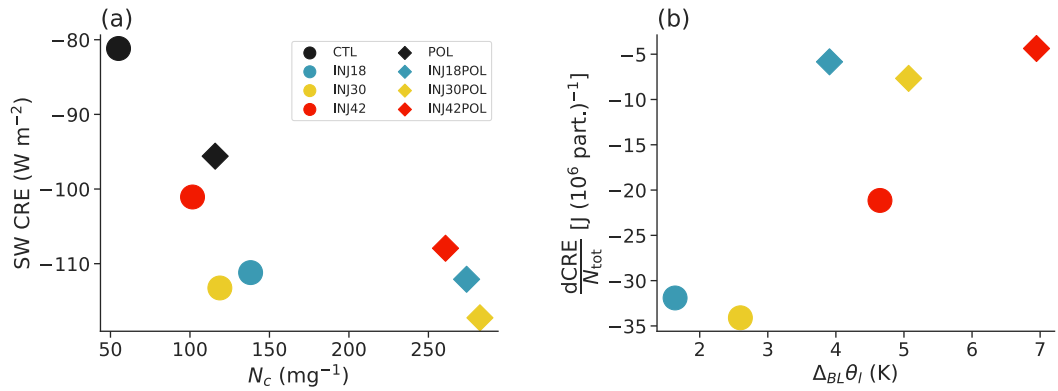

Figure 6. (a) Time-averaged shortwave cloud radiative effect (SW CRE) during 18–72 hr as a function of cloud droplet number concentration (N_c) for simulations with lower background aerosol concentrations (CTL, INJ18, INJ30, and INJ42; shown as dots) and higher background aerosol concentrations (POL, INJ18POL, INJ30POL, and INJ42POL; shown as diamonds). (b) Change in time-averaged SW CRE (INJ minus control, dCRE) expressed in Joules per injected particle, calculated as mean SW CRE × domain area × time / number of injected particles, plotted against the marine boundary layer stability ($\Delta_{BL}\theta_l$) averaged over the 12 hr after aerosol injection.

pattern of convergence in $<N_a>$ evolution across the plume runs indicates that whenever aerosols are injected, they tend to follow the established declining path of $<N_a>$ from earlier injections.

The above findings have significant implications for the impacts of aerosol injection timing on the SCT. The timing of aerosol injection is a conundrum: earlier injections facilitate greater aerosol transport to the stratocumulus cloud aloft due to stronger surface coupling, but the entrainment and accretion sinks of MBL aerosols act for a longer period of time, resulting in fewer aerosols remaining and thus diminishing their effect on cloud transitions. In contrast, later injections can retain more aerosols to influence the transition but encounter weakened aerosol vertical transport due to more decoupled MBL. Figure 4a indicates that the extent of these two ways that influence aerosol evolution is close, as seen in the overlapping decline of $<N_a>$ in INJ30 and INJ42 with that of INJ18. Consequently, the timing of aerosol injection has minimal impact on the SCT, and cloud properties (LCF and LWP in Figure 5) and MBL characteristics (not shown) remain largely consistent across INJ18, INJ30, and INJ42. While INJ30 and INJ42 show a slight increase in cloud deck persistence compared to INJ18 (∼1.5 hr, Figure 5a), this extension is less significant compared to the prolongation already seen in INJ18 (9 hr). Note that the stratocumulus cloud lifetime or the persistence of the cloud deck is measured as the time it takes for the initial LCF to decrease to 1/*e*.

Figure 6 shows the impact of injection timing on time-averaged CRE and the efficiency of MCB. Under clean background conditions, aerosol injections before 42 hr (INJ18 and INJ30) have similar cooling effects, whereas the injection at 42 hr yields a weaker cooling effect (Figures 5c and 6a). This reduction occurs mainly because the 42-hr injection is made after precipitation is already developed (Figure 5d), making part of the cooling effect associated with precipitation suppression no longer captured. Under polluted background conditions, where precipitation is minimal, the timing of aerosol injection or the MBL decoupling has little influence. This is also true for the impact of injection timing or decoupling on the efficiency of MCB (Figure 6b): injections performed before precipitation (if any) lead to little variation in MCB efficiency.

5. Aerosol Effects on the SCT

This section addresses the third question: How does surface aerosol injection affect cloud properties and CREs over the SCT with different background aerosol concentrations? Since changes in the timing of aerosol injection (before drizzle if any) lead to similar delays in the SCT and the MCB efficiency, we fix the injection time at the earliest point (18 hr). We then conduct a series of sensitivity runs by varying injection rates and background aerosol concentrations to enhance our insight into the efficiency of MCB through aerosol injection.

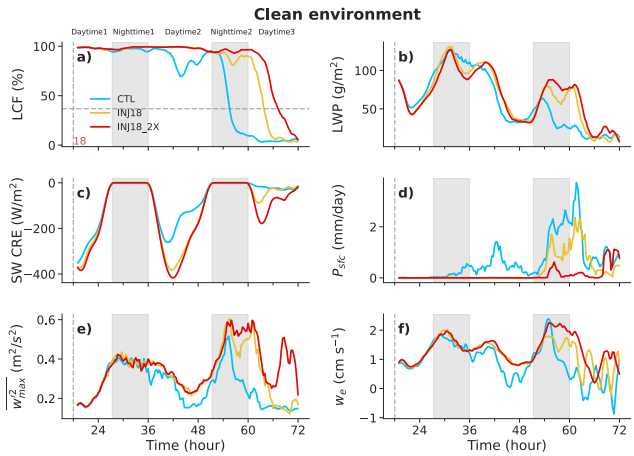

Figure 7. Time series of domain-mean (a) low-cloud fraction (LCF), (b) liquid water path, (c) shortwave cloud radiative effect, (d) surface precipitation rate, (e) maximum vertical velocity variance, and (f) entrainment rate for experiments CTL, INJ18, and INJ18_2X in clean environments. Gray boxes mark nighttime (7 p.m.–4 a.m. Local Time). The horizontal dashed line in panel (a) represents the value to which the initial LCF decreases by a factor of *e*.

5.1. Response of Cloud Evolution to Aerosols

5.1.1. Clean Environment

Figure 7 shows the time series of domain-mean LCF, LWP, surface precipitation, and MBL features for experiments CTL, INJ18, and INJ18_2X in clean environments. In the CTL run, the LCF first experiences a reduction to 60%, followed by a recovery, during Daytime1 (as designated in Figure 7a). This is overall consistent with GOES observations (see Figure 5 in Erfani et al. (2022b)), despite a larger minimum cloud fraction simulated (40% observed by GOES). Shortly after the recovery, the LCF decreases again until a total break-up of stratocumulus cloud decks, ending with cumulus clouds. This dissipation process (LCF continuously decreasing until below 20%) takes around 6 hr and is almost half the value of GOES observations. Erfani et al. (2022b) argued that the too-fast transition simulated by LES is likely due to too strong positive precipitation-aerosol-scavenging feedback in the prognostic aerosol scheme, manifested by persistently enhanced surface precipitation until exhausting LWP (Figures 7b and 7d).

When aerosols are injected into MBL, the lifetime of stratocumulus decks is notably extended by approximately 9 hr (see INJ18 vs. CTL in Figure 7a). This extension is primarily related to decreased precipitation during Nighttime2, suppressed by increased aerosols that slow the coalescence process (Figure 4f). Consequently, the onset of LWP depletion and MBL turbulence weakening is notably delayed (∼6 hr) during the same period. The suppression of precipitation during Daytime2 also contributes to the extension by enhancing LWP retention and elevating the peak of LWP before cloud breakup starts. An enhancement in entrainment is observed during Day2 (Daytime2 + Nighttime2) (Figure 7f), partly owing to the sedimentation-entrainment effect. As a result, the inversion height in INJ18 is continuously rising after 42 hr. Precipitation suppression by aerosol injection also results in the intensification of MBL turbulence (Figure 7e), leading to an increase in LCF (Figure 7a), consistent with Chun et al. (2023)'s findings. Next, we will delve into a process-level understanding of how aerosols affect the SCT transition.

To achieve that, the domain-mean LWP tendency is decomposed into five components influenced by cloud-top entrainment (*Ent*), cloud-base moisture fluxes (*Base*), large-scale subsidence (*Subs*), radiation (*Rad*), and precipitation (*Prec*), as illustrated in Figure 8. This decomposition is applicable only when cloud base and top heights of stratocumulus clouds can be determined. The decomposition is also more accurate under weaker drizzling conditions (Figure 8f). Before the onset of precipitation suppression (roughly at 30 hr), INJ18 shows a slight reduction in LWP, possibly because the cloud layer becomes less well-mixed or adiabatic after aerosol injection. Thereafter, precipitation is substantially suppressed, during which the *Prec*, *Ent*, and *Base* exhibit dominant impacts on LWP evolution over the *Subs* and *Rad*. The suppression of precipitation (*Prec*) moistens cloud layers, particularly during the middle of Daytime2 (see sky-blue vs. red lines in Figure 8c). The moistening effect is, however, partly counterbalanced by the changes in the *Ent* and *Base*. Overall, the moistening effect from the *Prec* predominates over the drying effects of the *Ent* and *Base*, which explains a net increase in LWP during Daytime2. This dominant moistening effect is expected to extend beyond cloud breakup in the CTL run, thereby prolonging the lifetime of the stratocumulus cloud deck observed in INJ18.

Doubling the injection rate extends the persistence of stratocumulus decks by another 3 hr, as shown by the comparison of red and yellow lines in Figure 7a. This extension in INJ18_2X, however, is more limited compared to INJ18 due primarily to the already substantial suppression of precipitation at the standard injection rate. With this saturation effect, we also see that prior to the cloud breakup (around 60 hr), the evolution of cloud properties, MBL characteristics, and LWP budget terms in INJ18_2X closely matches that in INJ18, except for a slight decrease in LWP during Day1.

5.1.2. Polluted Environment

Figure 9 illustrates how cloud evolution in polluted environments responds to aerosol injection. In comparison to CTL, POL exhibits a delayed SCT due to a dominant moistening effect induced by suppressed precipitation.

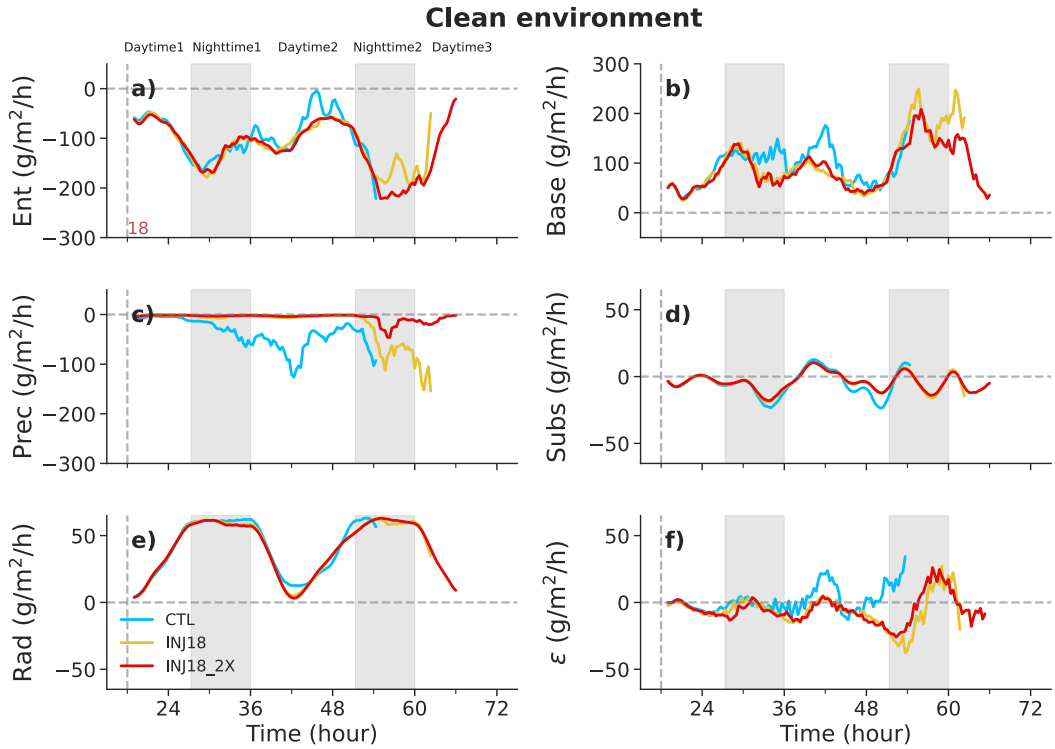

Figure 8. Time series of the domain-mean liquid water path (LWP) tendency due to (a) large-scale subsidence, (b) entrainment, (c) cloud-base turbulent fluxes, (d) radiation, and (e) precipitation for experiments CTL, INJ18, and INJ18_2X in clean environments. Panel (f) shows the actual LWP tendency minus the calculated LWP tendency. The time series of the actual LWP tendency is shown in Figure S4 of Supporting Information S1. Gray boxes mark nighttime (7 p.m.–4 a.m. Local Time).

When aerosols are injected into such a polluted MBL, the transition is extended by 2 hr (see yellow line in Figure 9a), and this trivial extension remains the same even when the injection rate is doubled.

The most pronounced effects of aerosol injection on the MBL in POL are observed during periods of drizzle, including substantial suppression of precipitation (Figure 9d), enhanced entrainment (Figure 9f) due to reduced sedimentation and increased cloud fraction and LWP, and a corresponding increase in MBL height (not shown). Outside the drizzling periods, aerosol injections exert minimal impact on those MBL processes quantified in Equation 1, as evidenced by the three overlapping lines in Figure 10. Due to the saturation effect of aerosols, INJ18POL and INJ18POL_2X show almost identical results. The exception is that INJ18POL_2X exhibits more significant LWP depletion possibly driven by evaporation when LWP exceeds 75 g/m^2 during the first half of the simulation. In summary, within a polluted MBL, both LCF and LWP show minor responses to aerosol injection, largely due to the limited effects of precipitation suppression. Prabhakaran et al. (2024) show that injected aerosols can notably delay the SCT in polluted systems. This difference is due to the existence of a relatively strong precipitation episode (>2 mm/day persisting over 6 hr) in their cases.

5.2. Response of CREs to Aerosols

The change in CRE or dCRE due to aerosol perturbation is associated with changes in in-cloud N_c, domain-mean LCF, and in-cloud LWP, according to Equation 2. Figure 11a shows the time evolution of the in-cloud N_c ratio between the plume runs and CTL in clean environments. In INJ18, the in-cloud N_c is generally doubled relative to CTL after aerosol injection and then slowly increases over the simulation before the onset of the SCT (around 51 hr). As a result, an evident cloud radiative cooling due to the Twomey effect is exhibited during Daytimes 1 and 2 (Figure 11e). LCF is primarily subject to MBL drizzling, and its increase in INJ18 occurs during Daytimes 2 and 3 when drizzle is significantly suppressed by injected aerosols (Figure 7a), causing a substantial cooling by reflecting more solar radiation, particularly for the duration in which more cloud fraction is sustained. This

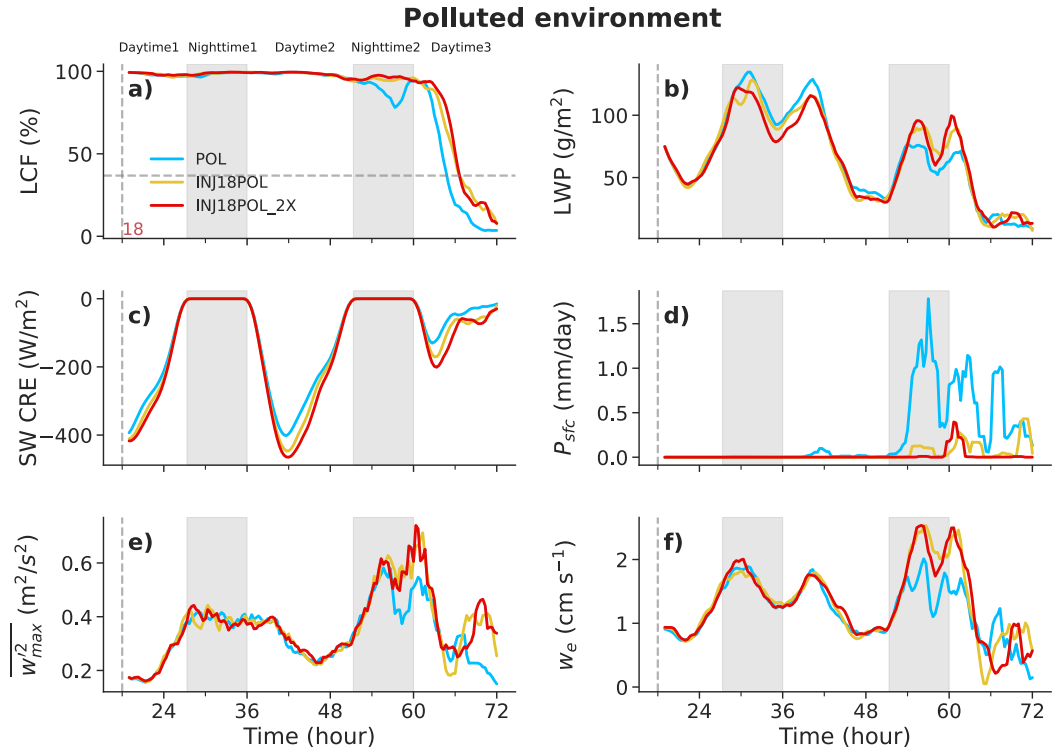

Figure 9. Same as Figure 7, but for polluted environments.

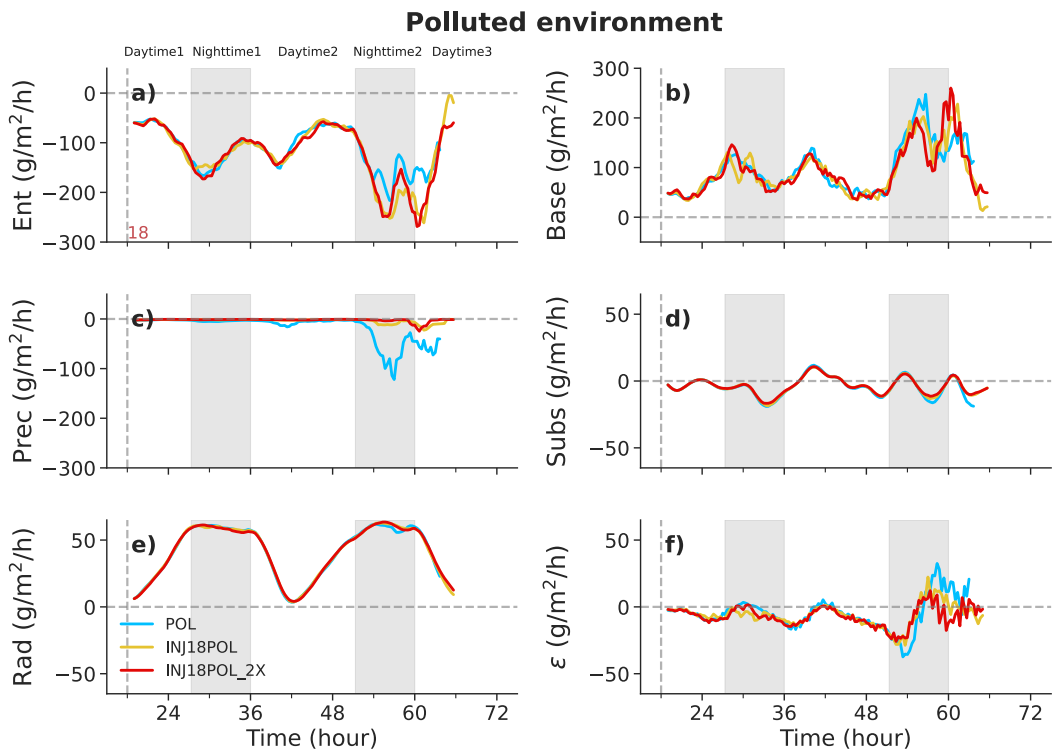

Figure 10. Same as Figure 8, but for polluted environments.

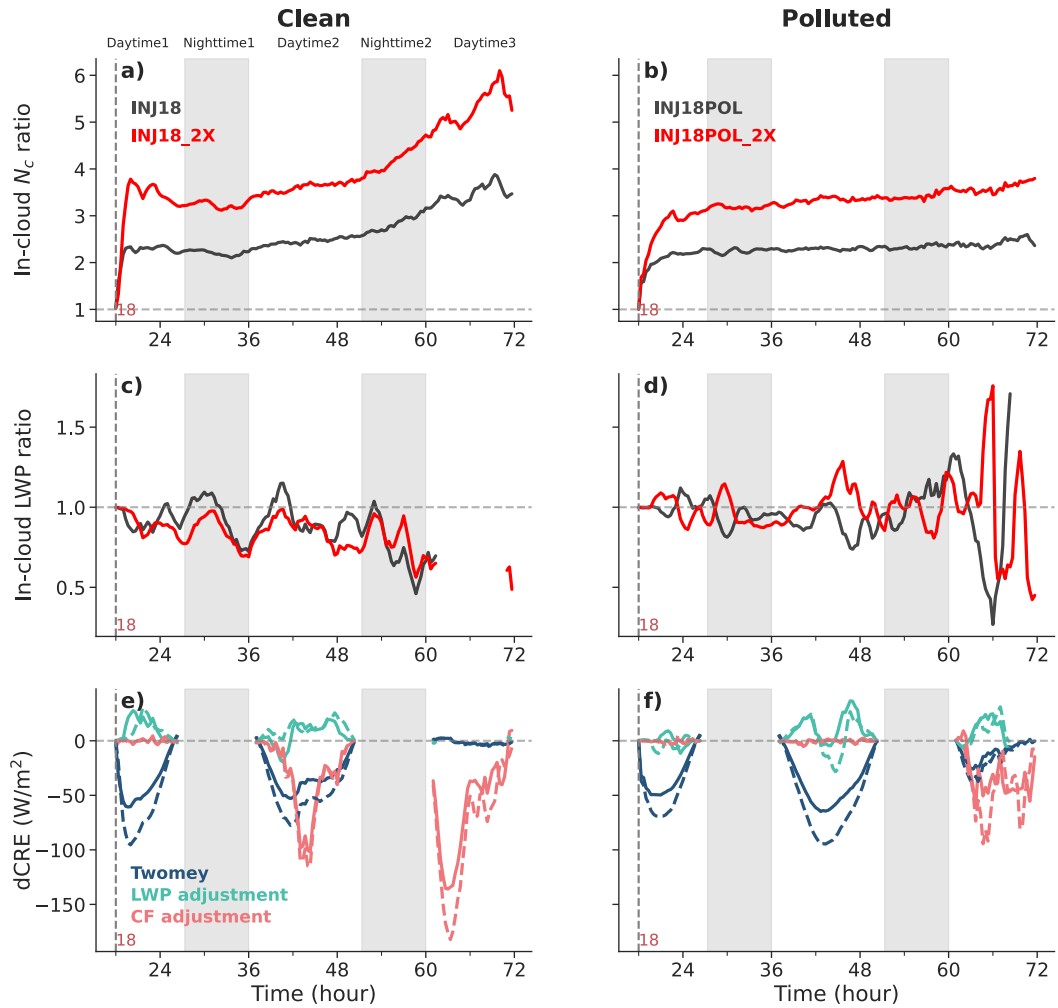

Figure 11. Time series of (a) the ratio of the perturbed to baseline in-cloud N_c, (c) the ratio of the perturbed to baseline in-cloud liquid water path (LWP), and (e) change in shortwave cloud radiative effects due to the Twomey effects, LWP adjustments, and cloud fraction (CF) adjustments, for INJ18 (solid lines) and INJ18_2X (dashed lines). Panels (b, d, and f) are the same but for polluted conditions (INJ18POL and INJ18POL_2X).

dominant cooling induced by cloud fraction adjustments is also seen in Chun et al. (2023) and Prabhakaran et al. (2024). As for the in-cloud LWP in INJ18 (Figure 11c), its depletion during Daytime2 is caused by increased entrainment drying. The decreased in-cloud LWP causes a warming effect, but its magnitude is much smaller compared to the cooling effect induced by the Twomey effect and cloud fraction adjustments due to relatively small LWP responses, in line with Prabhakaran et al. (2024); however, Chun et al. (2023) found a slight cooling effect for LWP adjustments. When doubling the aerosol injection rate (INJ18_2X), dCRE is not doubled correspondingly. The in-cloud N_c shows the most evident response, increased by ∼1.8 times referencing INJ18, yielding a roughly doubled cooling effect in INJ18_2X. However, the adjustments of LCF and in-cloud LWP are moderate, making the associated dCRE minor (see blue and green lines in Figure 11e).

In contrast, the responses of in-cloud properties and CREs exhibit different behaviors in polluted environments. The increases in in-cloud N_c in plume runs (INJ18POL and INJ18POL_2X) relative to POL equilibrate 3 hr after injection, as opposed to consistently increasing in-cloud N_c ratios in clean environments (Figure 11b). The latter is related to the decreased N_c in CTL, which is removed by precipitation. The cooling effects due to the Twomey effects dominate during Daytimes 1 and 2 in both INJ18POL and INJ18POL_2X. The changes in LCF in these plume runs only occur when cloud breakup is delayed, yielding cooling effects during Daytime3. Compared to its clean counterpart, INJ18POL shows no evident changes in in-cloud LWP during Daytime1, but they become

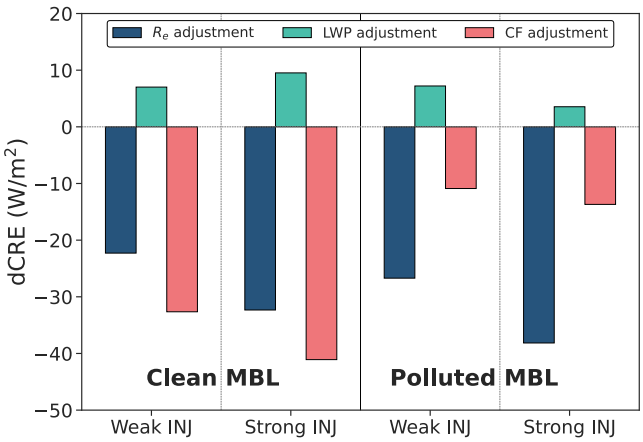

Figure 12. Changes in shortwave cloud radiative effects (dCRE) attributed to aerosol-induced adjustments in cloud effective radius (R_e) (also known as the Twomey effect), liquid water path (LWP), and cloud fraction (CF) under clean and polluted marine boundary layer (MBL) conditions. Weak and strong injections correspond to the standard and doubled injection strengths, respectively (i.e., INJ18 and INJ18_2X in clean MBLs, and INJ18POL and INJ18POL_2X in polluted MBLs).

noticeable during Daytimes 2 and 3, leading to small warming effects (Figure 11d). Similar to clean environments, dCRE due to the Twomey effect is most sensitive to aerosol injection rate.

Figure 12 summarizes dCRE (averaged throughout the simulation after aerosol injection) due to the Twomey effects, LWP adjustments, and cloud fraction adjustments under various scenarios. Overall, in response to aerosol injection, the Twomey effects and cloud fraction adjustments display evident cooling effects, while LWP adjustments show minor warming effects. The relative importance of these effects to dCRE is subject to background aerosol concentrations. In clean MBLs, cloud fraction adjustments exhibit the largest contribution to dCRE, followed by a slightly lower contribution from the Twomey effects, consistent with previous LES studies on MCB (Chun et al., 2023; Prabhakaran et al., 2024; Wang et al., 2011). The dominant cloud fraction adjustment in ACI forcing is also observed in the humid condition from satellite observations of volcanic eruptions (Chen et al., 2024). However, in polluted MBLs, the Twomey effects dominate, followed by halved contributions from cloud fraction adjustments. Wang et al. (2024) also found a more significant cloud fraction adjustment under clean conditions than under polluted conditions. The residual of dCRE decomposition terms (ζ) is summarized in Figure S6 of Supporting Information S1, showing a relatively large cooling residual in clean MBLs.

6. Discussion

The domain sizes of simulations have potential impacts on aerosol mixings and aerosol injection strategy (locations and number of point sources). H. Wang et al. (2011) and Prabhakaran et al. (2024) employed a large domain in their studies so that the effect of mesoscale circulations can be taken into account. Wang et al. (2011) found that the boundary-layer eddies do not mix CCN horizontally very efficiently, in contrast to efficiently mixed CCN in our study due to a small domain only ∼1/60 of their size. Prabhakaran et al. (2024) reported that under pristine conditions aerosol dispersal is more efficient due to transverse circulation driven by gradients in precipitation rates across the plume track. In addition to effects on aerosol mixing, the along-track and transverse gradients in CCN number concentration can invoke dynamic feedback in precipitating stratocumulus cases, which can impact clouds as well beyond the microphysical influences (Wang et al., 2011). A small domain was, however, adopted in our study, as it simplifies the injection strategies (e.g., only one source pointer used), lowers computing burden, and allows focusing on the impact of boundary layer eddies on aerosol vertical transport. Although our study does not consider the effect of mesoscale circulations, the key results are consistent with those of large domains (Chun et al., 2023; Prabhakaran et al., 2024; Wang et al., 2011), for example, the dominant impact of precipitation suppression on the SCT delay and the relative importance of adjustments in cloud properties along the SCT with different background aerosol concentrations, as discussed previously. These consistencies highlight the crucial role of boundary-layer eddies in interactions between surface aerosols and MBL clouds. The relative importance of MBL eddies and mesoscale circulations on aerosol mixings and associated ACI warrants future investigation.

In our study, the influence of injected aerosols on the SCT was investigated based on a case of initially clean, well-mixed MBL with relatively strong precipitation occurring later. Other cases, like an initially decoupled and polluted MBL (see Trajectory L10 in Erfani et al. (2022b)) and an initially well-mixed and weak drizzling MBL (Albrecht et al., 1995), might exhibit a different response to injected aerosols due to changed MBL structures and dynamics. It is also worth noting that injected particles here are accumulation mode aerosols, following the same lognormal distribution that represents the background CCN population. Injecting coarse mode aerosols such as dust particles, not explored yet, may help enhance Twomey effects and modify brightening efficiency, as they require lower supersaturation to be activated according to Köhler theory. Moreover, different large-scale meteorology may influence our results as well. For example, in an MBL with drier air beyond, LWP adjustments would be strengthened due to more efficient drying from the entrainment of overlying air (Ackerman et al., 2004).

7. Summary

This study investigated the impact of cloud-surface coupling on aerosol vertical mixing during the SCT using LESs. Aerosols were injected from the surface into the MBL at distinct times before the transition occurs to explore how different degrees of cloud-surface coupling impact the SCT, noting that clouds are more decoupled from the surface when moving toward warmer sea surfaces. By fixing the injection time, we further explored the impact of injected aerosols on cloud properties and CREs during the SCT by varying the aerosol injection rate and background aerosol concentrations.

Cloud-surface coupling is found to markedly influence the domain-mean aerosol transport from the subcloud layer to the stratocumulus layer, by modulating mixing within the MBL and the fractional area of buoyant updraft cores within the cumulus layer. Despite the significant role of coupling in aerosol vertical transport, the timing of aerosol injection (before drizzle if any) has little effect on the SCT and the efficiency of MCB. This results from two compensating effects: earlier injections enhance aerosol supply to the stratocumulus cloud base through relatively stronger cloud-surface coupling, but also experience greater depletion through prolonged entrainment and accretion, leading to similar aerosol number concentrations before the onset of SCT whenever aerosols are injected. We also find that in a clean MBL, aerosol injection significantly delays the SCT by effectively suppressing precipitation, which outweighs the increase in entrainment drying partly from sedimentation-entrainment effects, thereby sustaining cloud fraction. Conversely, in a polluted MBL, the influence of aerosol injection on the SCT is negligible due to the weakened precipitation suppression or saturated aerosol effects, akin to the scenario when aerosol injection rates are doubled in a clean MBL.

To gain deeper insight into changes in CRE (dCRE) due to aerosol perturbation, we decomposed them into three components due to the Twomey effect, LWP adjustments, and cloud fraction adjustments. The significance of these components to overall dCRE varies with background aerosol concentrations: in cleaner environments, cloud fraction adjustments contribute most significantly to dCRE (in the last day), whereas in polluted environments, Twomey effects are more dominant (in the first 2 days). These findings coincide with those of Chun et al. (2023), despite their results derived from idealized stratocumulus cases with fixed meteorological boundary conditions. These results highlight that suppressing precipitation as a means of sustaining cloud fraction (or extending the SCT) appears to be the most efficient way to enhance MCB in clean environments. Overall, our findings have critical implications for geoengineering strategies of MCB: (a) Injection timing (before drizzle if any) does not affect the SCT and MCB efficiency; (b) To achieve a more efficient MCB, it is suggested to inject aerosols into a clean MBL with strong precipitation occurring later, which can substantially enhance the cooling effect by suppressing precipitation and sustaining cloud fraction.

Conflict of Interest

The authors declare no conflicts of interest relevant to this study.

Data Availability Statement

Initial profiles, large-scale forcings, and aerosols used for our baseline simulations are available at Erfani et al. (2022a). Simulation outputs for our experiments can be accessed at Zhang et al. (2025).

Acknowledgments
This study is supported by the Department of Energy (DOE) Atmospheric System Research program (DESC0022919) and the National Science Foundation (AGS2126098). YZ is supported by the DOE Early Career grant (DE-SC0024185). We acknowledge high-performance computing support from Cheyenne (https://doi.org/10.5065/D6RX99HX; offline after 12/31/2023) and Derecho: HPE Cray EX System (https://doi.org/10.5065/qx9a-pg09) provided by NCAR's Computational and Information Systems Laboratory, sponsored by the National Science Foundation. We thank Peter Blossey for providing the SAM code that is coupled with a bulk aerosol scheme. ChatGPT was used to proof the manuscript.

References

Ackerman, A. S., Kirkpatrick, M. P., Stevens, D. E., & Toon, O. B. (2004). The impact of humidity above stratiform clouds on indirect aerosol climate forcing. *Nature*, *432*(7020), 1014–1017. https://doi.org/10.1038/nature03174

Albrecht, B., Ghate, V., Mohrmann, J., Wood, R., Zuidema, P., Bretherton, C., et al. (2019). Cloud system evolution in the trades (CSET): Following the evolution of boundary layer cloud systems with the NSF–NCAR GV. *Bulletin of the American Meteorological Society*, *100*(1), 93–121. https://doi.org/10.1175/BAMS-D-17-0180.1

Albrecht, B. A. (1989). Aerosols, cloud microphysics, and fractional cloudiness. *Science*, *245*(4923), 1227–1230. https://doi.org/10.1126/science.245.4923.1227

Albrecht, B. A., Bretherton, C., Johnson, D., Scubert, W. H., & Frisch, A. S. (1995). The Atlantic stratocumulus transition Experiment—astex. *Bulletin of the American Meteorological Society*, *76*(6), 889–904. https://doi.org/10.1175/1520-0477(1995)076<0889:TASTE>2.0.CO;2

Berner, A. H., Bretherton, C., & Wood, R. (2015). Large eddy simulation of ship tracks in the collapsed marine boundary layer: A case study from the Monterey area ship track experiment. *Atmospheric Chemistry and Physics*, *15*(10), 5851–5871. https://doi.org/10.5194/acp-15-5851-2015

Berner, A. H., Bretherton, C., Wood, R., & Muhlbauer, A. (2013). Marine boundary layer cloud regimes and POC formation in a CRM coupled to a bulk aerosol scheme. *Atmospheric Chemistry and Physics*, *13*(24), 12549–12572. https://doi.org/10.5194/acp-13-12549-2013

Bretherton, C., Blossey, P. N., & Jones, C. R. (2013). Mechanisms of marine low cloud sensitivity to idealized climate perturbations: A single-LES exploration extending the CGILS cases. *Journal of Advances in Modeling Earth Systems*, *5*(2), 316–337. https://doi.org/10.1002/jame.20019

Bretherton, C., Blossey, P. N., & Uchida, J. (2007). Cloud droplet sedimentation, entrainment efficiency, and subtropical stratocumulus albedo. *Geophysical Research Letters*, *34*(3). https://doi.org/10.1029/2006GL027648

Bretherton, C., Krueger, S. K., Wyant, M. C., Bechtold, P., Stevens, B., & Teixeira, J. (1999). A GCSS boundary-layer cloud model intercomparison study of the first ASTEX lagrangian experiment. *Boundary-Layer Meteorology*, *93*(3), 341–380. https://doi.org/10.1023/a:1002005429969

Bretherton, C., & Wyant, M. C. (1997). Moisture transport, lower-tropospheric stability, and decoupling of cloud-topped boundary layers. *Journal of the Atmospheric Sciences*, *54*(1), 148–167. https://doi.org/10.1175/1520-0469(1997)054<0148:MTLTSA>2.0.CO;2

Chen, Y., Haywood, J., Wang, Y., Malavelle, F., Jordan, G., Peace, A., et al. (2024). Substantial cooling effect from aerosol-induced increase in tropical marine cloud cover. *Nature Geoscience*, *17*(5), 404–410. https://doi.org/10.1038/s41561-024-01427-z

Chen, Y. S., Prabhakaran, P., Hoffmann, F., Kazil, J., Yamaguchi, T., & Feingold, G. (2025). Magnitude and timescale of liquid water path adjustments to cloud droplet number concentration perturbations for nocturnal non-precipitating marine stratocumulus. *Atmospheric Chemistry and Physics*, *25*(12), 6141–6159. https://doi.org/10.5194/acp-25-6141-2025

Christensen, M. W., Gettelman, A., Cermak, J., Dagan, G., Diamond, M., Douglas, A., et al. (2022). Opportunistic experiments to constrain aerosol effective radiative forcing. *Atmospheric Chemistry and Physics*, *22*(1), 641–674. https://doi.org/10.5194/acp-22-641-2022

Chun, J. Y., Wood, R., Blossey, P., & Doherty, S. J. (2023). Microphysical, macrophysical, and radiative responses of subtropical marine clouds to aerosol injections. *Atmospheric Chemistry and Physics*, *23*(2), 1345–1368. https://doi.org/10.5194/acp-23-1345-2023

Clarke, A. D., Owens, S. R., & Zhou, J. (2006). An ultrafine sea-salt flux from breaking waves: Implications for cloud condensation nuclei in the remote marine atmosphere. *Journal of Geophysical Research*, *111*(6). https://doi.org/10.1029/2005JD006565

Deardorff, J. W. (1976). On the entrainment rate of a stratocumulus-topped mixed layer. *Quarterly Journal of the Royal Meteorological Society*, *102*(433), 563–582. https://doi.org/10.1002/qj.49710243306

Deardorff, J. W. (1980). Stratocumulus-capped mixed layers derived from a three-dimensional model. *Boundary-Layer Meteorology*, *18*(4), 495–527. https://doi.org/10.1007/BF00119502

Dhandapani, C., Kaul, C. M., Pressel, K. G., Blossey, P. N., Wood, R., & Kulkarni, G. (2025). Sensitivities of large eddy simulations of aerosol plume transport and cloud response. *Journal of Advances in Modeling Earth Systems*, *17*(2), e2024MS004546. https://doi.org/10.1029/2024MS004546

Diamond, M. S., Director, H. M., Eastman, R., Possner, A., & Wood, R. (2020). Substantial cloud brightening from shipping in subtropical low clouds. *AGU Advances*, *1*(1), e2019AV000111. https://doi.org/10.1029/2019av000111

Eastman, R., & Wood, R. (2018). The competing effects of stability and humidity on subtropical stratocumulus entrainment and cloud evolution from a Lagrangian perspective. *Journal of the Atmospheric Sciences*, *75*(8), 2563–2578. https://doi.org/10.1175/JAS-D-18-0030.1

Erfani, E., Blossey, P., Wood, R., Mohrmann, J., Doherty, S., Wyant, M., & Kuan-Ting, O. (2022a). Data for paper: Simulating aerosol lifecycle impacts on the subtropical stratocumulus-to-cumulus transition using large-eddy simulations (v1) [Dataset]. *Zenodo*. https://doi.org/10.5281/zenodo.7005166

Erfani, E., Blossey, P., Wood, R., Mohrmann, J., Doherty, S. J., Wyant, M., & Kuan-Ting, O. (2022b). Simulating aerosol lifecycle impacts on the subtropical stratocumulus-to-cumulus transition using large-eddy simulations. *Journal of Geophysical Research: Atmospheres*, *127*(21), e2022JD037258. https://doi.org/10.1029/2022JD037258

Gelaro, R., McCarty, W., Suárez, M. J., Todling, R., Molod, A., Takacs, L., et al. (2017). The modern-era retrospective analysis for research and applications, version 2 (MERRA-2). *Journal of Climate*, *30*(14), 5419–5454. https://doi.org/10.1175/JCLI-D-16-0758.1

Hartmann, D. L., & Short, D. A. (1980). On the use of earth radiation budget statistics for studies of clouds and climate. *Journal of the Atmospheric Sciences*, *37*(6), 1233–1250. https://doi.org/10.1175/1520-0469(1980)037<1233:OTUOER>2.0.CO;2

Hersbach, H., Bell, B., Berrisford, P., Hirahara, S., Horányi, A., Muñoz-Sabater, J., et al. (2020). The ERA5 global reanalysis. *Quarterly Journal of the Royal Meteorological Society*, *146*(730), 1999–2049. https://doi.org/10.1002/qj.3803

Iacono, M. J., Delamere, J. S., Mlawer, E. J., Shephard, M. W., Clough, S. A., & Collins, W. D. (2008). Radiative forcing by long-lived greenhouse gases: Calculations with the AER radiative transfer models. *Journal of Geophysical Research*, *113*(13). https://doi.org/10.1029/2008JD009944

Igel, A. L. (2024). Processes controlling the entrainment and liquid water response to aerosol perturbations in nonprecipitating Stratocumulus clouds. *Journal of the Atmospheric Sciences*, *81*(9), 1605–1616. https://doi.org/10.1175/JAS-D-23-0238.1

Khairoutdinov, M., & Randall, D. A. (2003). Cloud resolving modeling of the ARM summer 1997 IOP: Model formulation, results, uncertainties, and sensitivities. *Journal of the Atmospheric Sciences*, *60*(4), 607–625. https://doi.org/10.1175/1520-0469(2003)060<0607:CRMOTA>2.0.CO;2

Klein, S. A., & Hartmann, D. L. (1993). The seasonal cycle of low stratiform clouds. *Journal of Climate*, *6*(8), 1587–1606. https://doi.org/10.1175/1520-0442(1993)006<1587:TSCOLS>2.0.CO;2

Latham, J. (1990). Control of global warming? *Nature*, *347*(6291), 339–340. https://doi.org/10.1038/347339b0

Li, X. Y., Wang, H., Chen, J., Endo, S., George, G., Cairns, B., et al. (2022). Large-Eddy simulations of marine boundary layer clouds associated with cold-air outbreaks during the ACTIVATE campaign. Part I: Case setup and sensitivities to large-scale forcings. *Journal of the Atmospheric Sciences*, *79*(1), 73–100. https://doi.org/10.1175/JAS-D-21-0123.1

Morrison, H., & Grabowski, W. W. (2008). Modeling supersaturation and subgrid-scale mixing with two-moment bulk warm microphysics. *Journal of the Atmospheric Sciences*, *65*(3), 792–812. https://doi.org/10.1175/2007JAS2374.1

Possner, A., Wang, H., Wood, R., Caldeira, K., & P. Ackerman, T. (2018). The efficacy of aerosol-cloud radiative perturbations from near-surface emissions in deep open-cell stratocumuli. *Atmospheric Chemistry and Physics*, *18*(23), 17475–17488. https://doi.org/10.5194/acp-18-17475-2018

Prabhakaran, P., Hoffmann, F., & Feingold, G. (2024). Effects of intermittent aerosol forcing on the stratocumulus-to-cumulus transition. *Atmospheric Chemistry and Physics*, *24*(3), 1919–1937. https://doi.org/10.5194/acp-24-1919-2024

Rieck, M., Nuijens, L., & Stevens, B. (2012). Marine boundary layer cloud feedbacks in a constant relative humidity atmosphere. *Journal of the Atmospheric Sciences*, *69*(8), 2538–2550. https://doi.org/10.1175/JAS-D-11-0203.1

Sandu, I., & Stevens, B. (2011). On the factors modulating the stratocumulus to cumulus transitions. *Journal of the Atmospheric Sciences*, *68*(9), 1865–1881. https://doi.org/10.1175/2011JAS3614.1

Scott, R. C., Myers, T. A., Norris, J. R., Zelinka, M. D., Klein, S. A., Sun, M., & Doelling, D. R. (2020). Observed sensitivity of low-cloud radiative effects to meteorological perturbations over the global oceans. *Journal of Climate*, *33*(18), 7717–7734. https://doi.org/10.1175/JCLI-D-19-1028.1

Slingo, A. (1990). Sensitivity of the Earth's radiation budget to changes in low clouds. *Nature*, *343*(6253), 49–51. https://doi.org/10.1038/343049a0

Twomey, S. (1977). The influence of pollution on the shortwave Albedo of clouds. *Journal of the Atmospheric Sciences*, *34*(7), 1149–1152. https://doi.org/10.1175/1520-0469(1977)034<1149:TIOPOT>2.0.CO;2

van der Dussen, J. J., De Roode, S. R., & Siebesma, A. P. (2014). Factors controlling rapid stratocumulus cloud thinning. *Journal of the Atmospheric Sciences*, *71*(2), 655–664. https://doi.org/10.1175/JAS-D-13-0114.1

van der Dussen, J. J., De Roode, S. R., & Siebesma, A. P. (2016). How large-scale subsidence affects stratocumulus transitions. *Atmospheric Chemistry and Physics*, *16*(2), 691–701. https://doi.org/10.5194/acp-16-691-2016

Wang, H., Rasch, P. J., & Feingold, G. (2011). Manipulating marine stratocumulus cloud amount and albedo: A process-modelling study of aerosol-cloud-precipitation interactions in response to injection of cloud condensation nuclei. *Atmospheric Chemistry and Physics*, *11*(9), 4237–4249. https://doi.org/10.5194/acp-11-4237-2011

Wang, X., Mao, F., Zhu, Y., Rosenfeld, D., Pan, Z., Zang, L., et al. (2024). Hidden large aerosol-driven cloud cover effect over high-latitude ocean. *Journal of Geophysical Research: Atmospheres*, *129*(13), 1–12. https://doi.org/10.1029/2023JD039312

Williams, A. S., & Igel, A. L. (2021). Cloud top radiative cooling rate drives non-precipitating stratiform cloud responses to aerosol concentration. *Geophysical Research Letters*, *48*(18), e2021GL094740. https://doi.org/10.1029/2021GL094740

Wood, R. (2021). Assessing the potential efficacy of marine cloud brightening for cooling Earth using a simple heuristic model. *Atmospheric Chemistry and Physics*, *21*(19), 14507–14533. https://doi.org/10.5194/acp-21-14507-2021

Wood, R., & Bretherton, C. (2004). Boundary layer depth, entrainment, and decoupling in the cloud-capped subtropical and tropical marine boundary layer. *Journal of Climate*, *17*(18), 3576–3588. https://doi.org/10.1175/1520-0442(2004)017<3576:BLDEAD>2.0.CO;2

Wyant, M. C., Bretherton, C., Rand, H. A., & Stevens, D. E. (1997). Numerical simulations and a conceptual model of the stratocumulus to trade cumulus transition. *Journal of the Atmospheric Sciences*, *54*(1), 168–192. https://doi.org/10.1175/1520-0469(1997)054<0168:NSAACM>2.0.CO;2

Yamaguchi, T., Feingold, G., & Kazil, J. (2017). Stratocumulus to cumulus transition by drizzle. *Journal of Advances in Modeling Earth Systems*, *9*(6), 2333–2349. https://doi.org/10.1002/2017ms001104

Zhang, H., Zheng, Y., Lee, S. S., & Li, Z. (2023). Surface-atmosphere decoupling prolongs cloud lifetime under warm advection due to reduced entrainment drying. *Geophysical Research Letters*, *50*(10), e2022GL101663. https://doi.org/10.1029/2022GL101663

Zhang, H., Zheng, Y., & Li, Z. (2024). Evaluation of stratocumulus evolution under contrasting temperature advections in CESM2 through a Lagrangian framework. *Geophysical Research Letters*, *51*(4), e2023GL106856. https://doi.org/10.1029/2023GL106856

Zhang, H., Zheng, Y., & Li, Z. (2025). Dataset for paper titled "Influence of surface aerosol injection on stratocumulus-to-cumulus transition: Cloud-surface coupling and background aerosol concentrations" (V2.0) [Dataset]. *Zenodo*. https://doi.org/10.5281/zenodo.17872471

Zheng, Y., Zhang, H., Rosenfeld, D., Lee, S.-S., Su, T., & Li, Z. (2021). Idealized large-eddy simulations of stratocumulus advecting over cold water. Part I: Boundary layer decoupling. *Journal of the Atmospheric Sciences*, *78*(12), 4089–4102. https://doi.org/10.1175/JAS-D-21-0108.1